RECENT RESULTS FROM THE S-POD TRAP SYSTEMS ON THE STABILITY OF INTENSE HADRON BEAMS*

H. Okamoto#, K. Ito, K. Fukushima, T. Okano,
AdSM, Hiroshima University, Higashi-Hiroshima 739-8530, Japan

Abstract

S-POD (Simulator of Particle Orbit Dynamics) is a tabletop experimental apparatus developed at Hiroshima University for systematic studies of various beam dynamic effects in modern particle accelerators. This novel experiment is based on an isomorphism between the basic equations governing the collective motion of a non-neutral plasma in a trap and that of a charged-particle beam in an alternating-gradient (AG) focusing channel. The system is particularly useful in exploring space-charge-induced collective phenomena whose accurate study is often troublesome in practice or quite time-consuming to simulate even with high-performance computers. This paper addresses recent experimental results on the stability of intense hadron beams traveling through long periodic AG transport channels. Emphasis is placed upon coherent resonances that occur depending on the lattice design, beam intensity, error fields, etc.

INTRODUCTION

It is often difficult to perform systematic investigation of intense beam behavior not only in an experimental way but also in a numerical way. Experimentally, the overall lattice structure of a large machine is not changeable once it is constructed. Other fundamental parameters such as tunes, beam density, etc. are also not very flexible in general as long as we rely on real accelerators or beam transport channels. Although these parameters can be chosen freely in numerical simulations, high-precision tracking of charged particles interacting each other via the Coulomb fields is quite time-consuming even with modern parallel computers whenever the beam intensity is high. To overcome or lighten these practical difficulties that we face in fundamental beam dynamics studies, we proposed the concept "Laboratory Accelerator Physics" where the tabletop system called "S-POD" is employed instead of a large-scale machine to *experimentally* simulate the collective motion of high-intensity beams [1,2]. This accelerator-free experiment allows us to explore a wide range of parameter space simply by controlling the AC and DC voltages applied to the electrodes. Since everything is stationary in the laboratory frame, high-resolution measurements can readily be done and we do not have to worry about radio-activation due to heavy particle losses. S-POD experiment, indeed, has practical limitations [3], but it gives us useful insight into intense beam dynamics easily and quickly.

*Work supported in part by a Grant-in-Aid for Scientific Research, Japan Society for Promotion of Science.
#okamoto@sci.hiroshima-u.ac.jp

Three independent S-POD systems based on linear Paul traps (LPT) [4] were designed and constructed at Hiroshima University, which have been applied to different beam-physics purposes [2,5-7]. In this paper, we summarize recent experimental results from S-POD II and III on collective resonance instability depending on AG lattices. As mentioned above, such an experimental study cannot be conducted systematically in any real machine whose lattice structure is fixed. We here control the radio-frequency (rf) waveform of quadrupole focusing to emulate the beam behavior in several standard AG lattices involving doublet and FDDF sequence.

S-POD

S-POD is composed mainly of a compact LPT, DC and AC power sources, a vacuum system, and a personal computer that controls a series of measurements and data saving. Figure 1 shows a side view of a typical multi-sectioned LPT employed for S-POD. Four cylindrical rods are symmetrically placed to generate the rf quadrupole potential for strong transverse focusing of ions. The transverse motion of an ion confined in a LPT is governed by the Hamiltonian [1]

$$H = \frac{p_x^2 + p_y^2}{2} + \frac{1}{2} K_{\mathrm{rf}}(\tau)(x^2 - y^2) + I\phi, \qquad (1)$$

where the independent variable is $\tau = ct$ with c being the speed of light, I is a constant depending on the ion species, and the function $K_{\mathrm{rf}}(\tau)$ is proportional to the rf voltage applied to the quadrupole rods. Since the collective Coulomb potential ϕ and the time-evolution of the ion distribution in phase space obey the Vlasov-Poisson equations, this many-body system is physically equivalent to a charged-particle beam traveling through an AG

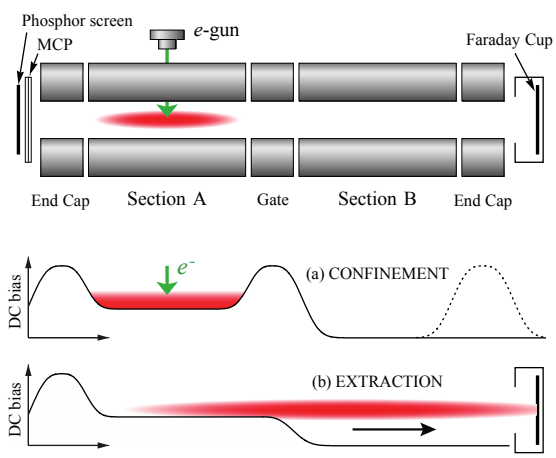

Figure 1: Typical measurement steps [8].

ISBN 978-3-95450-173-1

transport channel. We can thus study the fundamental features of intense beams by observing the collective behavior of an ion plasma in a LPT. Unlike the case of actual beam transport channels with many Q-magnets, the AG focusing function $K_{\mathrm{rf}}(\tau)$ in S-POD is controllable over a wide range without any mechanical change to the trap geometry; all we need is to change the waveform of the rf voltage. It is possible to introduce imbalance between the horizontal and vertical focusing strengths if necessary, so that we can independently adjust the two bare tunes.

S-POD II and III are both operated at the frequency of 1 MHz (in the case of standard sinusoidal or doublet focusing). The ion species chosen for the present experiment is $^{40}\mathrm{Ar}^{+}$. Then, the maximum rf amplitude required to survey the full tune space is less than around 100 V. As illustrated in Fig. 1, the quadrupole electrodes of the LPT are divided into five electrically isolated pieces in the axial direction. In addition to the transverse rf voltages, we add proper DC bias voltages to these five quadrupole sections to form a longitudinal potential well. After a necessary experimental procedure is completed, one of the longitudinal potential barriers is dropped to extract the plasma toward the Faraday cup or the MCP detector on the other side.

DOUBLET FOCUSING

The rf power generator of S-POD has been designed to produce a wide range of stepwise waveforms. While the sinusoidal waveform is commonly used in regular LPTs, we have tried more complex waveforms including doublet, triplet, FDDF, etc [8]. Figure 2 shows a doublet waveform that has the quadrupole filling factor of 0.25. The distance from QF (focusing pulse) to QD (defocusing pulse) has been set equal to that from QD to QF in this example. The number of $^{40}\mathrm{Ar}^{+}$ ions surviving after 10 ms (10^4 rf periods) in this AG potential is plotted in Fig. 3 as a function of the bare phase advance per single doublet cell. Since the horizontal and vertical focusing are symmetric, the phase advances $(\sigma_{0x}, \sigma_{0y})$ in both directions are identical; namely, $\sigma_{0x} = \sigma_{0y} (\equiv \sigma_0)$. We find three clear instability regions, all of which shift to the higher σ_0 side as the initial plasma density increases. Essentially the same stop-band distribution has been repeatedly observed in past S-POD experiments where the sinusoidal rf waveform was employed for transverse ion confinement [5-7]. According to a Vlasov theory [9] as well as past numerical work [10], the instability of the linear collective mode should be responsible for major ion losses near $\sigma_0 \approx 90$ [deg]. The other two stop bands near $\sigma_0 \approx 60$ and 120 [deg] are probably due to the third-order resonances. Since the instabilities near $\sigma_0 \approx 60$ and 90 [deg] are driven by the space-charge potential rather than external nonlinear error fields, these collective resonances are considerably weakened or even almost disappear at low density. We have carried out a number of stop-band measurements using various doublet waveforms with different geometric factors. We then observe the same stop band distribution as indicated in Fig. 3 as long as the symmetric transverse focusing ($\sigma_{0x} = \sigma_{0y}$) is assumed.

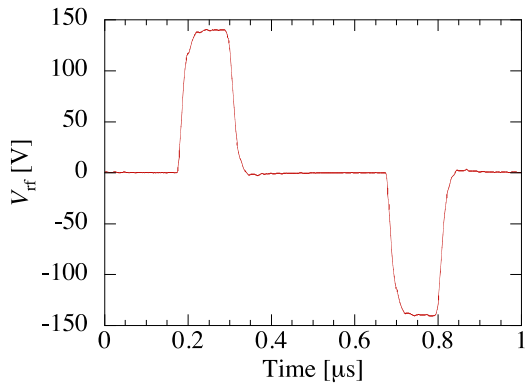

Figure 2: A doublet-type waveform produced by the rf power source of S-POD II.

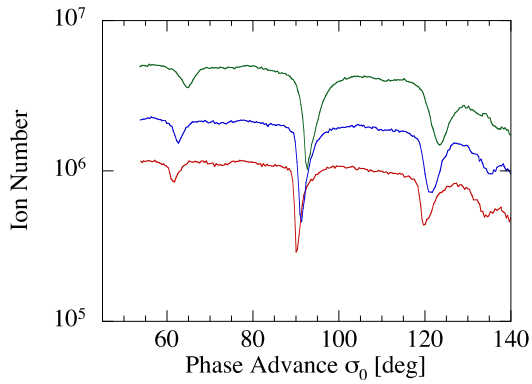

Figure 3: Resonance instability bands corresponding to the doublet focusing in Fig. 2.

COUPLING RESONANCE

The ion losses near $\sigma_0 \approx 60$ and 90 [deg] in Fig. 3 should be caused by purely horizontal and vertical resonances overlapping each other. For instance, at $\sigma_0 \approx 90$ [deg], we have a possibility of relatively low order (2nd- and 4th-order) resonances independently in both transverse directions; namely, the conditions of primary resonances are given by $2\sigma_{0x} \approx 180$ [deg], $2\sigma_{0y} \approx 180$ [deg], $4\sigma_{0x} \approx 360$ [deg], and $4\sigma_{0y} \approx 360$ while the former two resonances become prominent only at high intensity [9]. Each of these stop bands splits into two parts when we introduce weak asymmetry in the transverse focusing strengths such that $\sigma_{0x} \neq \sigma_{0y}$ and then plot the stop band distribution as a function of either σ_{0x} or σ_{0y}. On the other hand, coupling resonance lines that depend simultaneously on σ_{0x} and σ_{0y} may also be created if sufficiently strong error fields are present. The resonance condition at zero intensity is given by $m\sigma_{0x} \pm n\sigma_{0y} = (\text{integer}) \times 360°$ for the driving field of

ISBN 978-3-95450-173-1

the form $x^m y^n$ where m and n are positive integers. In the case of the lowest-order nonlinearity, i.e. sexupole, $(m, n) = (1, 2)$ or $(2, 1)$. To confirm the existence of such coupling resonance lines, we employed S-POD III driven by the sinusoidal rf waveform, instead of the doublet type, for the sake of simplicity. Figure 4 is the phase-advance diagrams experimentally obtained at different ion densities. The ion loss rate after a certain storage period is color-coded in the region of relatively high phase advances where we expect the occurrence of nonlinear coupling resonances [11]. The two third-order sum resonance lines can be identified while the forth-order difference resonance line $2\sigma_{0x} - 2\sigma_{0y} = 0$ is invisible in this data. We recognize the stop-band shifts depending on the plasma intensity. Recent S-POD experiments as well as 2D Vlasov analysis suggest that at high beam intensity, coupling resonance is expected to occur under the condition

$$m(\sigma_{0x} - \Delta\sigma_x) \pm n(\sigma_{0y} - \Delta\sigma_y) = (\text{integer}) \times 360°, \quad (2)$$

where $\Delta\sigma_x$ and $\Delta\sigma_y$ are the phase-advance shifts induced by the Coulomb potential. If this condition is correct, the vertical (or horizontal) shift of a coupling resonance line in the phase-advance diagram depends on the combination of the integers m and n. For example, when $(m, n) = (2, 1)$ and $\Delta\sigma_x \approx \Delta\sigma_y$, the space-charge-induced shift of the sum resonance line is three times larger than that of the difference resonance. When $m = n$, the difference resonance line does not move depending on the plasma density (as long as $\Delta\sigma_x \approx \Delta\sigma_y$). In the case of a circular machine with the lattice superperiodicity of N_{sp}, the coupling resonance condition corresponding to Eq. (2) can be expressed as

$$m(\nu_{0x} - \Delta\nu_x) \pm n(\nu_{0y} - \Delta\nu_y) = kN_{sp}, \quad (3)$$

where k is an integer, and (ν_{0x}, ν_{0y}) are the transverse bare tunes depressed by the amount of $(\Delta\nu_x, \Delta\nu_y)$ at high intensity.

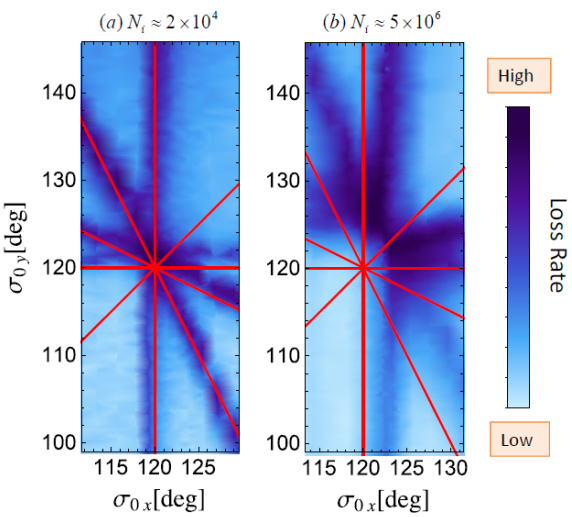

Figure 4: Resonance instability lines of sinusoidal focusing measured at different initial ion densities.

FDDF SEQUENCE

The FDDF (or FFDD) waveform is another popular lattice often adopted in modern accelerators. One such example is the UNILAC at GSI [12]. Although the unit cell contains four quadrupoles (two are focusing and the other two defocusing in one transverse plane), we reasonably expect that the overall resonance behavior should be similar to that of the doublet focusing. Recent S-POD experiments actually revealed that the stop band distribution of the FFDD lattice is the same as what we observe in Fig. 3. Three instability bands are found near $\sigma_0 \approx 60$, 90, and 120 [deg]. The stop band at $\sigma_0 \approx 90$ [deg] usually gives rise to the most severe ion losses provided the initial plasma density is high. However, as already mentioned, this instability becomes quite weak at low density unless a non-negligible source of fourth-order external driving force exists.

Highly Symmetric Ring

The three-stop-band feature as shown in Fig. 3 should be more or less universal among long linear transport channels whose structures are simple repetition of short focusing cells like FODO, symmetric doublet, and FFDD. In contrast, the resonance feature can be more complex in a circular machine because the focusing period is generally much longer. Each superperiod often contains several or more unit focusing blocks. The stored beam receives strictly periodic kicks every turn, even including imperfection fields. Such complex nature of a large closed system can make the stop-band distribution essentially different from that in Fig. 3.

Let us consider a circular machine consisting of N FDDF cells [13]. According to our past experience with S-POD, the condition of the transverse collective resonance excited independently in either the horizontal or vertical direction by the m-th order space-charge force is likely to have the form [9]

$$m(\nu_{0x(0y)} - \Delta\nu_{x(y)}) \approx \frac{kN_{sp}}{2}, \quad (4)$$

where the coherent tune shifts $\Delta\nu_{x(y)}$ depend on the order number m. Sacherer first pointed out theoretically that $\Delta\nu_{x(y)}$ is somewhat smaller for a lower-order resonance at a specific beam density [14]. As for the coupling resonance driven by the potential $x^m y^n$, the resonance condition (3) should hold.

As an example, we assume $N = 50$. If all 50 FDDF cells are perfectly identical, N_{sp} is also equal to 50. We then predict from Eq. (4) that the three stop bands as in Fig. 3 will appear at the tunes slightly above $50/6$, $50/4$, and $50/3$ in both transverse directions. The corresponding S-POD experiment was performed which resulted in the stop band distribution of Fig. 5(a) where $\nu_{0x} = \nu_{0y} (\equiv \nu_0)$ for simplicity. The number of ions initially stored in the trap is either 10^5 or 10^6. The ordinate represents the number of ions surviving after 100 turns around the 50-fold

ISBN 978-3-95450-173-1

symmetric ring. We observe three instability regions as expected.

Effect of Lattice Symmetry Breaking

The proton synchrotron (PS) at CERN is composed of 50 FDDF cells [15], similarly to the example taken in the last section. Therefore, three stop bands in Fig. 5(a) must be found also at CERN-PS near the bare tunes $\nu_{0x(0y)} = 50/6,\ 50/4$, and $50/3$ at high beam intensity even without imperfection fields. The actual focusing period around the ring is, however, not necessarily 50, namely, $N_{sp} \neq N$, but the lattice functions may be less symmetric depending on the choice of the tunes and other parameters. For instance, we here look into the case where the external driving force has 10-fold symmetry around the ring; namely, $N = 50$ but $N_{sp} = 10$. A single lattice superperiod then contains five FDDF blocks. Such type of lattice symmetry breaking has been considered in a possible new optics of PS to ensure a larger distance from nearby nonlinear resonance lines [16]. Among a wide variety of ways to reduce the symmetry of the rf focusing force, in the present study we took the waveform as illustrated in Fig. 6. Each superperiodic cell consists of four identical FDDF blocks plus one more FDDF with a slightly different geometric factor. This long focusing wave repeats 10 times every turn around the ring. The corresponding stop-band distribution measured with S-POD II is shown in Fig. 5(b). In this experiment, we changed the quadrupole filling factor of the fifth FDDF block by 2% compared to the other four blocks (that have the filling factor of 0.5). The focusing and defocusing pulse shapes were chosen identical so that $\nu_{0x} = \nu_{0y} (\equiv \nu_0)$. In addition to the three stop bands, several more unstable regions appear due to the reduction of the lattice symmetry. Specifically, rather severe instabilities are newly excited near $\nu_0 \approx 5$, 10, 15, and 20. It is interesting to see that at least two independent ion-loss mechanisms are present within each of these new instability regions; there is always a relatively wide instability band accompanied by very sharp and heavy ion losses on the low tune side. We notice that the sharp stop bands do not move much depending on the ion density. Another series of S-POD experiments have demonstrated that these stop bands are widened as we enhance the perturbation to the fifth FDDF cell in each superperiod.

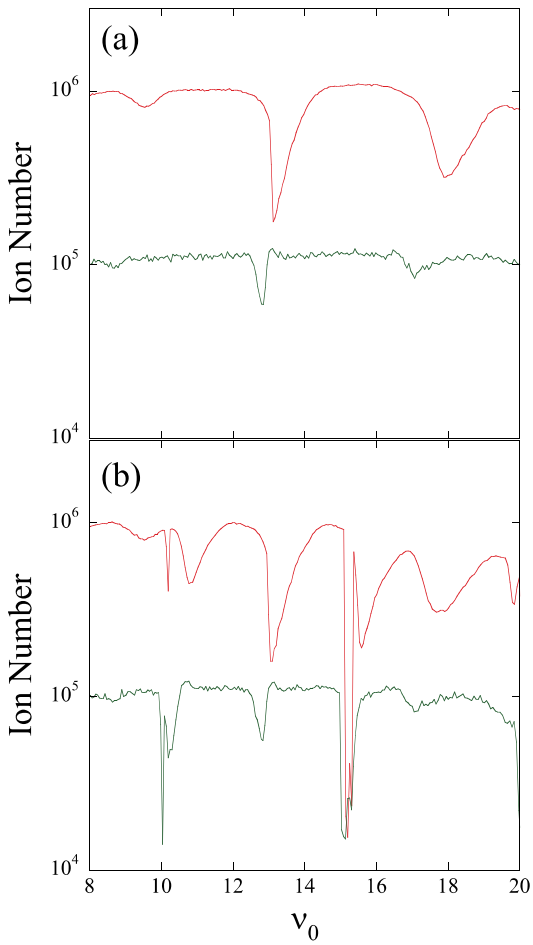

Figure 5: Resonance instability bands in a closed AG lattice consisting of 50 FDDF cells. (a) 50-fold symmetric case where all FDDF cells are identical. (b) 10-fold symmetric case where the pulse widths in every five FDDF cells are weakly perturbed as indicated in Fig. 6. The horizontal and vertical bare tunes are set equal in both cases.

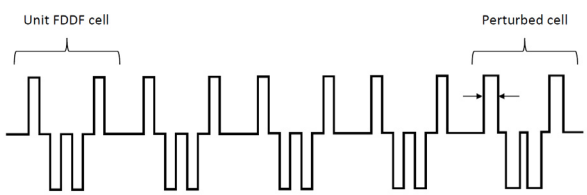

Figure 6: FDDF waveform with a perturbed cell.

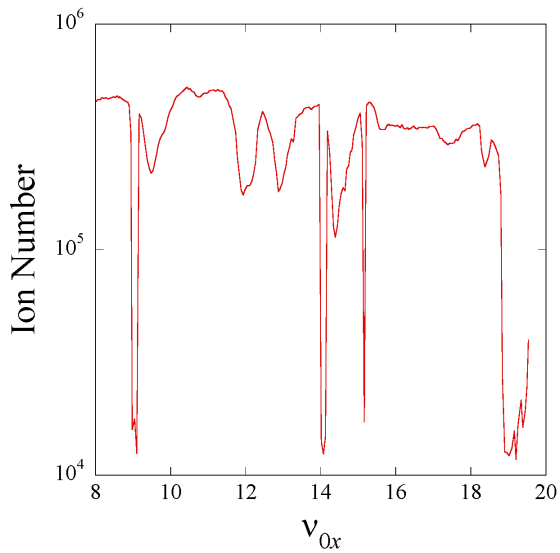

Figure 7: Resonance instability bands in the 10-fold symmetric lattice considered in Fig. 5(b). The two transverse tunes are not equal here but slightly different satisfying the relation $\nu_{0y} = \nu_{0x} + 0.02$.

ISBN 978-3-95450-173-1

It is also important to ask what happens when the transverse tunes are unequal (which corresponds to possible operating conditions of PS). To answer this question, we slightly modified all 50 FDDF pulses in an asymmetric way to develop imbalance between the horizontal and vertical focusing forces. Figure 7 shows the stop-band distribution obtained under the condition $\nu_{0y} = \nu_{0x} + 0.02$. Note that the measured data are plotted as a function of the vertical bare tune ν_{0x}. We confirm that the major stop bands in Fig. 5(b) split into two instability bands. This implies that most stop bands observed under the symmetric focusing condition $\nu_{0x} = \nu_{0y}$ have been created by two independent (horizontal and vertical) resonances overlapping at the same tune. The two sharp ion losses at $\nu_{0x} \approx 14$ and 15 in Fig. 7 probably originate from the narrow stop band at $\nu_0 \approx 15$ in Fig. 5. Since the abscissa of Fig. 7 is ν_{0x}, we assume that the ion losses staying at $\nu_{0x} \approx 15$ are due to horizontal instability while those shifted to $\nu_{0x} \approx 14$ occur vertically. On the other hand, it appears as if the narrow band at $\nu_{0x} \approx 10$ in Fig. 5(b) moved to $\nu_{0x} \approx 9$ without splitting, but we believe that there should still be the horizontal instability band at $\nu_{0x} \approx 10$ (which was too narrow to be detected in this experiment). In fact, we found very sharp instability at $\nu_{0x} \approx 10$ in another experiment performed under $\nu_{0y} = \nu_{0x} + 0.05$.

SUMMARY

The S-POD systems at Hiroshima University have been employed to explore fundamental beam dynamics issues in particle accelerators. In the present experimental study, we focused on transverse resonance instability caused by the periodic nature of AG focusing lattices. Several standard AG waveforms, such as sinusoid, doublet, and FDDF, was taken to demonstrate how such instability arises depending on particle density, bare tunes, and lattice symmetry breaking. It has been verified that the stop-band distributions are similar in long transport channels simply repeating any of these short, symmetric AG waveforms. We always encounter the distribution as depicted in Fig. 3, no matter what waveform geometric factors are chosen for doublet and FDDF. Needless to say, the stop-band distribution becomes much more complex when a unit lattice period contains not one but many AG focusing blocks of non-identical geometries. In any case, the coherent resonance condition in Eq. (4) seems to roughly explain the locations of major horizontal and vertical stop bands observed at high beam density. (At low density, the factor $1/2$ on the right hand side should be omitted.) Provided relatively strong nonlinear coupling potentials are present, we also expect the sum and/or difference resonances excited under the condition of Eq. (3). The existence of such coupling resonance lines was confirmed in S-POD III using the sinusoidal focusing waveform.

An interesting stop-band behavior has been found when a highly symmetric closed lattice is perturbed to have lower symmetry (Fig. 5). The symmetry breaking excites additional instability regions, each of which often includes a very narrow stop band and a wider one on the right. The origin of such double stop bands that appear side by side is presently unclear. While preliminary particle-in-cell simulations suggest that nonlinear driving fields may be responsible for the excitation of the sharp stop bands, we still need further careful investigation to reach a definitive conclusion on this issue. We are now planning to develop a unique multipole LPT that enables us to control the time structure and strengths of low-order nonlinearity independently of the primary quadrupole focusing potential [17].

REFERENCES

[1] H. Okamoto and H. Tanaka, Nucl. Instrum. Meth. A **437**, 178 (1999).
[2] H. Okamoto *et al.*, Nucl. Instrum. Meth. A **733**, 119 (2014).
[3] The S-POD experiment described here is based on linear Paul traps that utilize only electric fields for particle confinement. It is thus impossible to exactly reproduce *dispersive* effects induced by dipole magnetic fields in circular machines.
[4] P. K. Ghosh, *Ion Traps* (Oxford Science, Oxford, 1995) and references therein.
[5] S. Ohtsubo *et al.*, Phys. Rev. ST Accel. Beams **13**, 044201 (2010).
[6] H. Takeuchi *et al.*, Phys. Rev. ST Accel. Beams **15**, 074201 (2012).
[7] K. Fukushima *et al.*, Nucl. Instrum. Meth. A **733**, 18 (2014).
[8] H. Okamoto *et al.*, FRXAA01, IPAC'14, Dresden, Germany, June 2014, p. 4052 (2014).
[9] H. Okamoto and K. Yokoya, Nucl. Instrum. Meth. A **482**, 51 (2002).
[10] See, e.g., M. Reiser, *Theory and Design of Charged Particle Beams*, John Wiley & Sons, New York (1994), and references therein.
[11] The ion storage period in the low-intensity experiment (left figure) was 100 μs while we extended the period to 1 ms at high intensity (right figure) to enhance the loss rate.
[12] L. Groening *et al.*, Phys. Rev. Lett. **102**, 234801 (2009).
[13] We here ignore the effect from bending magnets.
[14] F. J. Sacherer, Ph.D thesis, Lawrence Radiation Laboratory [Report No. UCRL-18454, 1968].
[15] R. Wasef *et al.*, WEPEA070, IPAC'13, Shanghai, China, May 2013, p. 2669 (2013).
[16] S. Machida, private communication.
[17] H. Okamoto, Y. Wada, R. Takai, Nucl. Instrum. Meth. A **485**, 244 (2002).

ISBN 978-3-95450-173-1